Pergamon

PII: S0301-9322(96)00082-1

Int. J. Multiphase Flow Vol. 23, No. 3, pp. 455–471, 1997

Printed in Great Britain
0301-9322/97 $17.00 + 0.00

ANALYSIS OF PARTICLE MOTION IN A VERY SHALLOW FLUIDIZED BED

U. SCHAFLINGER[1], T. AIHARA[2], T. GRUBER[1], U. WEINGERL[1], T. OHARA[2] and W. SCHNEIDER[1]

[1]Institute of Fluid Dynamics and Heat Transfer, Technical University Vienna, Wiedner Haupstraße 7, A-1040 Vienna, Austria

[2]Institute of Fluid Science, Tohoku University, 2-1-1 Katahira, Aoba-ku, Sendai 980-77, Japan

(Received 6 March 1996; in revised form 30 October 1996)

Abstract—It is well known that heat transfer characteristics can be improved by immersing the heat exchanger tubes into a fluidized bed. However, conventional fluidized beds are rather unstable and the comparatively large bed height causes a high pressure drop. To address this problem, one of the authors developed a very shallow fluidized bed heat exchanger which is composed of a horizontal array of tubes and a special designed multislit distributer that produces several two-phase jets. The solid particles carried in the jet impinge against the tubes and cause continuous defrosting by abrading ice formation. Here we shall present theoretical predictions for the flow properties within the jet, the impingement rate against the tube and calculations of the granular flow of particles on the inclined bottom chute that feeds the solids back into the jet. The theoretical models are based on experimental observations and data which we also present here. © 1997 Elsevier Science Ltd. All rights reserved.

Key Words: defrosting, fluidized beds, granular flow

1. INTRODUCTION

Usually, humidity of air produces a thick layer of frost on conventional finned tube heat exchangers of heat pump and LNG-gasification systems. The frost layer reduces heat transfer, increases pressure loss and eventually causes total failure of the system.

Within the last decades several authors studied the frosting mechanism and the resulting heat transfer (Yamakawa *et al.* 1972; Hayashi *et al.* 1977; Seki *et al.* 1985; Aoki *et al.* 1985). More recently, Fukusako *et al.* (1985, 1989), and Torikoshi *et al.* (1990) have investigated the heat-transfer characteristics due to frosting of horizontal tubes immersed into a fluidized bed. This technique utilizes solid particle impingement onto frost layers and one can expect effective defrosting and an increase in heat transfer.

Here we study experimentally and theoretically the particle motion in a very shallow fluidized bed heat exchanger. The heat exchanger is composed of a horizontal array of tubes and a special two-dimensional multislit distributor producing several gas-solid particle jets impinging on each tube (Aihara *et al.* 1988; Muruyama *et al.* 1988, 1989). Since the system under investigation has been presented in great detail in Aihara *et al.* (1995), we shall just describe the main features here. Figure 1 shows a sketch of just one tube, the pertinent two-phase jet, the orifice and the inclined bottom walls which feed back the solid particles into the jet. For our purposes we divide the whole flow field into five regions (figure 1):

(1) mixing region,
(2) two-phase jet region,
(3) impinging region,
(4) surroundings,
(5) granular flow,

which are all interrelated but for the sake of simplicity are treated separately in this paper.

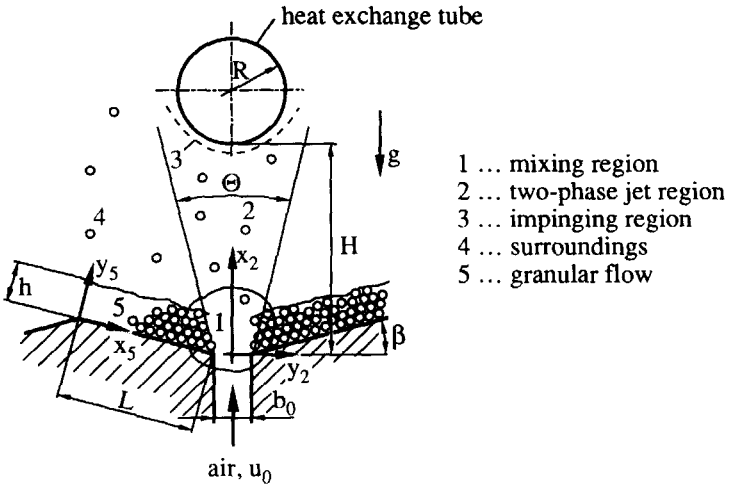

Figure 1. Sketch of the flow field. $L = 23$ mm, $H = 40$ mm, $R = 10$ mm, $\beta = 15^\circ$, $b_0 = 7$ mm, $\Theta = 28^\circ$.

By means of high speed video recordings, we first measure the particle-velocities on the inclined bottom walls (figure 1, region 5). This information provides the diagrams for the main particle velocity at three different locations and an estimate for the appropriate granular temperature. The video recordings also help us to estimate the spreading angle of the jet and the particle velocity inside the jet. This data enables us to calculate the flow characteristics of the sliding particles on the bottom walls, the particle flux inside the jet and the average impingement rate of particle on the tube. The theoretical investigation of the granular flow on a chute is a direct application of a model suggested by Johnson *et al.* (1990) while the calculation of the two-phase jet is based on global conservation of momentum (Laats and Frishman 1970; Schneider 1985). In the mixing region 1 (see figure 1) the mass flux of particles in the granular bed towards the jet is assumed to be independent of crosswise direction y_5 which causes the solids mass flux in the jet to linearly increase from zero to its final value. The actual defrosting mechanism as well as the surroundings of the jet have not yet been studied in detail and are subject to further investigations.

2. EXPERIMENTAL RESULTS

Using a high speed video film of a single jet (2250 frames/s) we measured first the velocity profiles of glass beads moving down the two-dimensional chute. Particles used in the experiments were glass beads with diameter $d_p = 1.5$ mm and density $\rho_p = 2400$ kg/m^3. Experiments were recorded for 17 different superficial velocities u_s in a range from 1.24 to 5.02 m/s. The velocity profiles were measured at three distinct positions (figure 2) for four different superficial velocities† (1.47, 2.26, 3.07 and 4.50 m/s). Evaluation of the video was made possibly by a transparent sheet with a 5 mm-grid which was placed on the video screen. This made it possible to trace a distinct particle over a distance of roughly 200 frames which equal a length of approximately 3 mm in the real experiment. For each profile the velocity of about 80 spheres was determined. Since the width of the gap was 7 mm in the real experiment and 46 mm on the screen, scaling was possible. Due to the resolution of the monitor, the actual position of a single sphere could be measured within ± 1 mm on the screen which led to a maximum error of $\pm 10\%$. It is possible that the velocities were slightly underestimated systematically as the glass beads observed were those moving close to the side plates of the set-up. In order to obtain a block average velocity u_{5a}, the arithmetic average was calculated of particle velocities within layers of 0.8 particle diameters d. Eventually, the granular temperature $u_5'^2$ was calculated as the fluctuations in u_5.

At relatively low superficial velocities $u_s = 1.24$ and 1.47 m/s the corresponding jets did not have sufficient energy to drag the glass beads up to the tube. The two-phase jet broke down and the

†For our experimental setup the relationship between the superficial velocity u_s and the jet velocity at the orifice u_0 is simply given by $u_0 = 7.14\ u_s$.

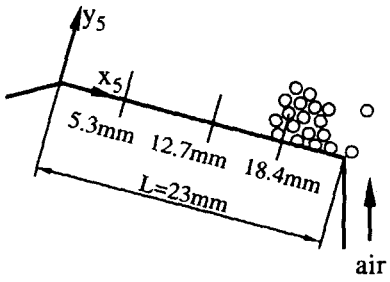

Figure 2. Positions for measuring the particle velocity.

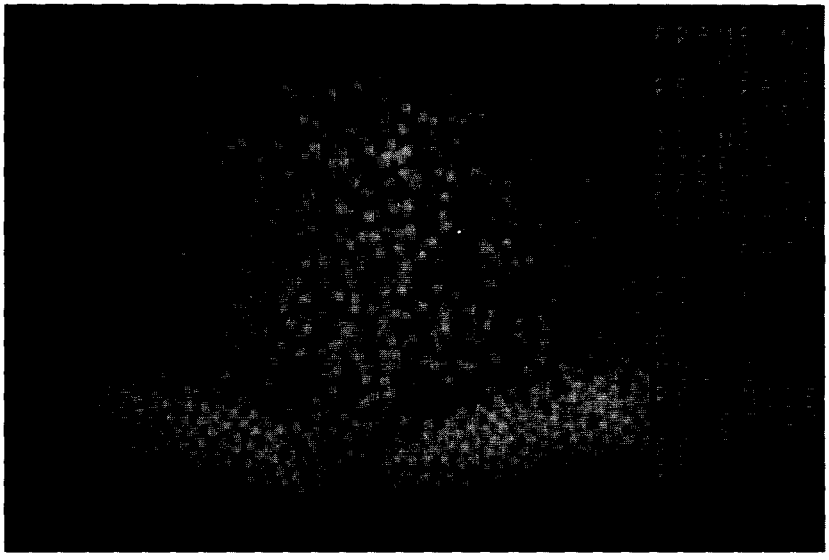

Figure 3. Experimental observation. $u_s = 1.47$ m/s.

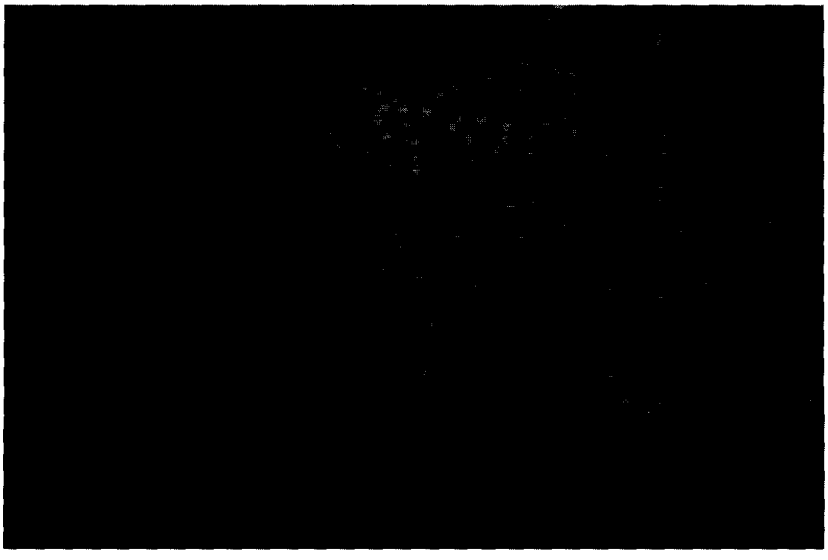

Figure 4. Experimental observation. $u_s = 2.26$ m/s.

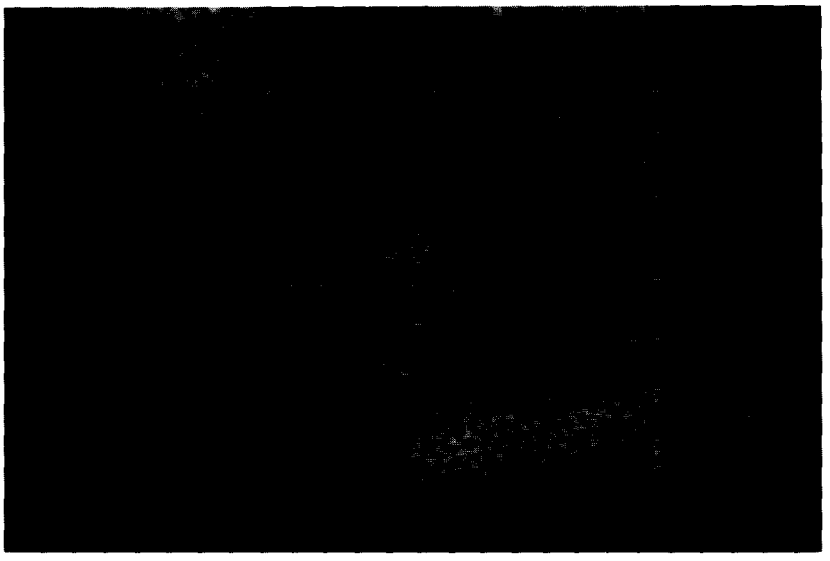

Figure 5. Experimental observation. $u_s = 3.07$ m/s.

particles formed a mushroom-like shape (figure 3) with slight spouting on top. The corresponding spreading angle of the jet was measured as $\Theta \sim 45°$. Occasionally, the glass beads did not slide uniformly down the slope and clusters of particles moved slower than adjacent particles. In the case of small superficial velocities the upper layers of sliding particles moved clearly faster than the lower ones (figure 7).

With increasing superficial velocity, i.e. $u_s = 1.76$ to 3.07 m/s, the glass beads were almost uniformly distributed in the whole area between the bottom and the tubes (figures 4 and 5) which led to the assumption that the volume concentrations of solid particles α_2 and α_4 are the same inside the jet region 2 and in the surroundings (region 4) (see figure 1) if $u_s \geqslant 1.76$ m/s. The spreading angle of the two-phase jet was estimated at $\Theta \sim 28°$.

The above mentioned clustering of glass beads did not occur for larger values of u_s, i.e. $u_s = 2.76$–3.07 m/s.

A further increase in u_s, i.e. $u_s = 3.27$–5.02 m/s, caused the jets to strongly oscillate in the plane of observation (figure 6). A distinct frequency could not be estimated from the video-film since the recording time was too short.

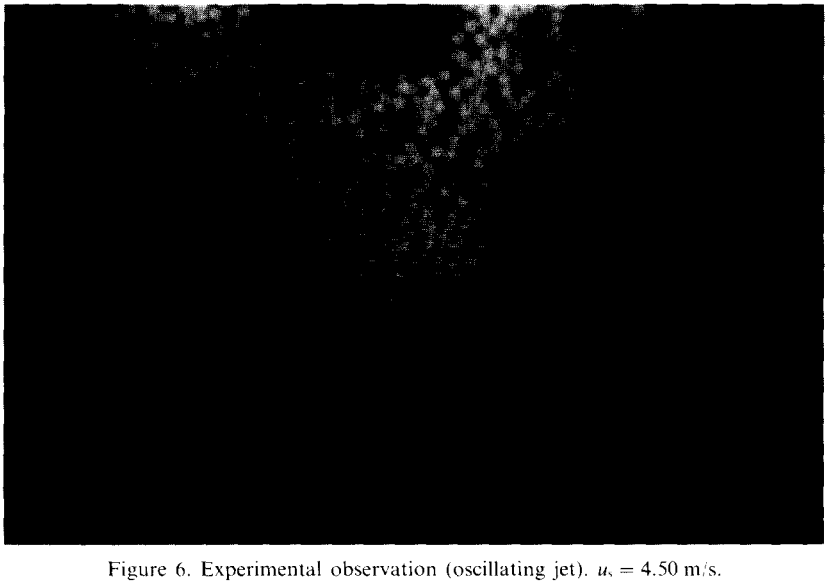

Figure 6. Experimental observation (oscillating jet). $u_s = 4.50$ m/s.

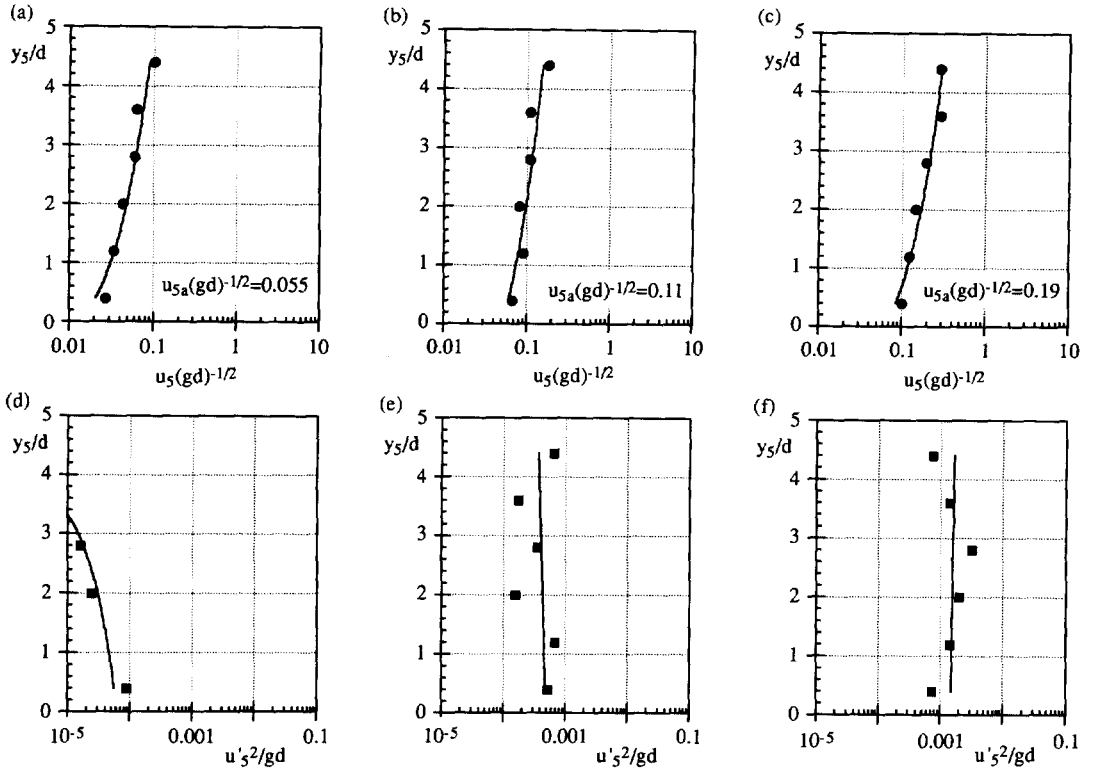

Figure 7. Measurements (u_s = 1.47 m/s). (a) particle velocity at x_5 = 5.3 mm; (b) particle velocity at x_5 = 12.7 mm; (c) particle velocity at x_5 = 18.4 mm; (d) granular temperature at x_5 = 5.3 mm; (e) granular temperature at x_5 = 12.7 mm; (f) granular temperature at x_5 = 18.4 mm.

At low superficial velocities the sliding particles slightly accelerated while moving towards the jet (figures 7 and 8). With increasing u_s, however, the velocity inside the granular bed became almost independent of the location in x_5-direction (figures 9 and 10). We observed unstable jet conditions for a superficial velocity u_s = 4.5 m/s. In this case we were not able to accurately measure the particle velocity distribution $u_5(y_5)$ at x_5/L = 0.23 with L being the total length of the chute.

As a general result we found that the average velocity profiles are almost linear with a distinct slip velocity on the bottom and maximum velocity on top (figures 7–10). In most cases the granular temperatures $u_5'^2$ (figures 7–10) are largest on top. Occasionally, however, they show an inverse trend (figure 7d, e) probably caused by the clustering of particles. In figure 11 the average velocity u_{5a} of the particles is plotted vs the superficial velocity u_s. Enhancing u_s from 1.46 to 4.5 m/s caused the appropriate average velocity u_{5a} to increase approximately as much as three times.

Using high speed video frames we also determined the particle velocity distribution of the solid particles inside the two-phase jet in a very similar manner as described above. Figure 12 shows non-dimensionalized measured particle velocities u_s/u_0 at two different locations x_2/b_0. The symbol b_0 refers to the width of the orifice (see figure 1) and in figure 12 the symbol x_v denotes the virtual origin of the jet. The solid curves shown in figure 12 are Gaussian fits.

3. TWO-PHASE JET

Here we investigate, by theoretical means, a plane turbulent two-phase jet in which the volume concentration of particles α_2 is very small whereas the mass fraction of solids is of order unity. The model presented below is based on conservation of overall momentum and on the assumption that no particles cross the edges of the jet (Zierfuß and Schneider 1992). This means that the particle mass flux remains constant in the jet above the mixing region (Laats and Frishman 1970).

Figure 13 sketches the jet region. Conservation of momentum yields:

$$\frac{\mathrm{d}}{\mathrm{d}x_2}\left[(1-\alpha_2)\rho_f b u_{fc}^2 2\int_0^{1/2}\left(\frac{u_f}{u_{fc}}\right)^2 \mathrm{d}\frac{y_2}{b}\right] + \frac{\mathrm{d}}{\mathrm{d}x_2}\left[\alpha_2\rho_p b u_{pc}^2 2\int_0^{1/2}\left(\frac{u_p}{u_{pc}}\right)^2 \mathrm{d}\frac{y_2}{b}\right] + (\alpha_2-\alpha_4)\rho_p b g = 0, \quad [1]$$

where the density is denoted by ρ, the symbol b is the width of the jet and u signifies the velocity in x_2 direction. The subscript f indicates fluid properties, while the index p refers to the solid particles. Properties at the centerline are marked with an additional subscript c. Since the presence of solid particles causes a significant change in the turbulence structure of the carrier phase and thus reduces the gas turbulence kinetic energy (Mostafa *et al.*, 1989), momentum transfer between the two phases due to interaction by drag and gravity forces can be written as:

$$\frac{\mathrm{d}}{\mathrm{d}x_2}\left[\alpha_2\rho_p b u_{pc}^2 2\int_0^{1/2}\left(\frac{u_p}{u_{pc}}\right)^2 \mathrm{d}\frac{y_2}{b}\right] = \alpha_2\rho_f\frac{3}{4d}c_{d_2}(u_{fc}-u_{pc})^2 2\int_0^{1/2}\left(\frac{u_f-u_p}{u_{fc}-u_{pc}}\right)^2 \mathrm{d}\frac{y_2}{b} - (1-\alpha_4)\alpha_2\rho_p b g. \quad [2]$$

The last term on the right hand side of [2] represents the gravity force acting on the particle phase, reduced by possible buoyancy of the surroundings. The drag coefficient c_{d_2} is given by the empirical relationship employed by Richardson and Zaki (1954)

$$c_{d_2} = c_d(1-\alpha_2)^{-n}, \quad [3]$$

where c_d is the drag coefficient of a single particle in pure fluid. For fluidized beds the exponent $n = 2.39$ (Wallis 1969). For the problem under investigation, however, an actual value of n is not yet known. In our case we assumed $c_d = 0.4$, which requires a Reynolds number larger than 1000 and hence an air velocity larger than 7 m/s for glass particles with a diameter $d = 1.55$ mm. This condition was practically always fulfilled. For an approximate value $\alpha_2 \sim 0.05$, [3] yields $c_{d_2} = 0.5$.

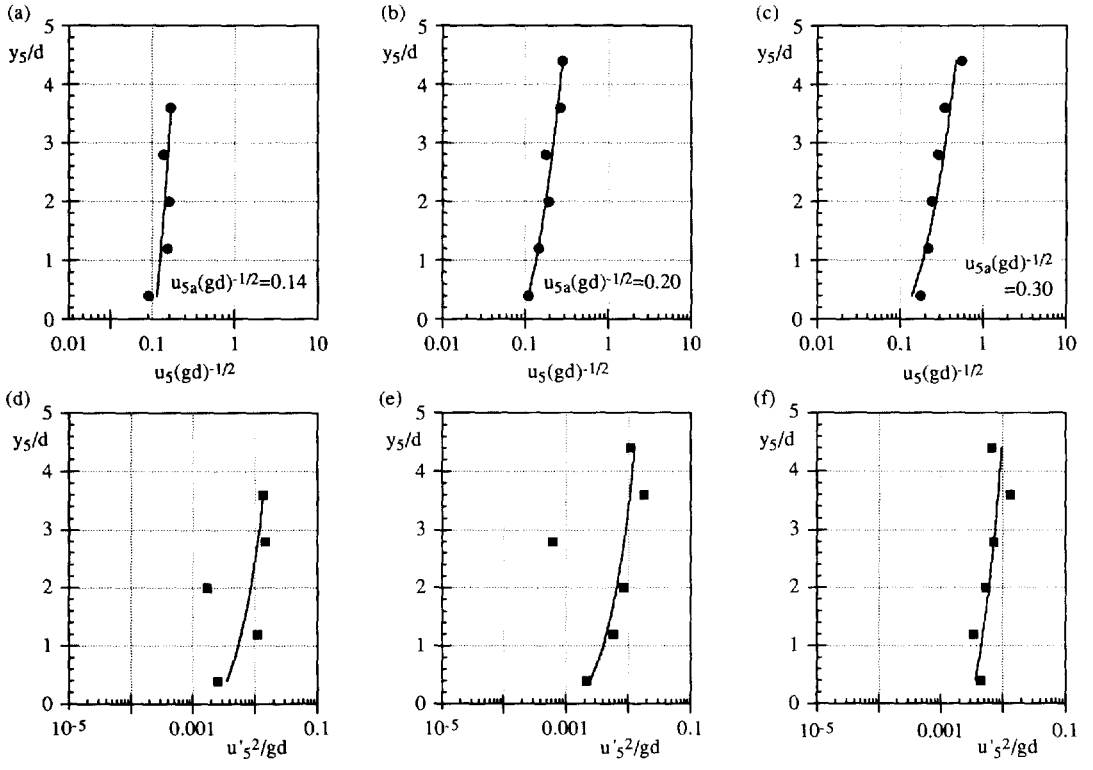

Figure 8. Measurements ($u_\infty = 2.26$ m/s). (a) particle velocity at $x_5 = 5.3$ mm; (b) particle velocity at $x_5 = 12.7$ mm; (c) particle velocity at $x_5 = 18.4$ mm; (d) granular temperature at $x_5 = 5.3$ mm; (e) granular temperature at $x_5 = 12.7$ mm; (f) granular temperature at $x_5 = 18.4$ mm.

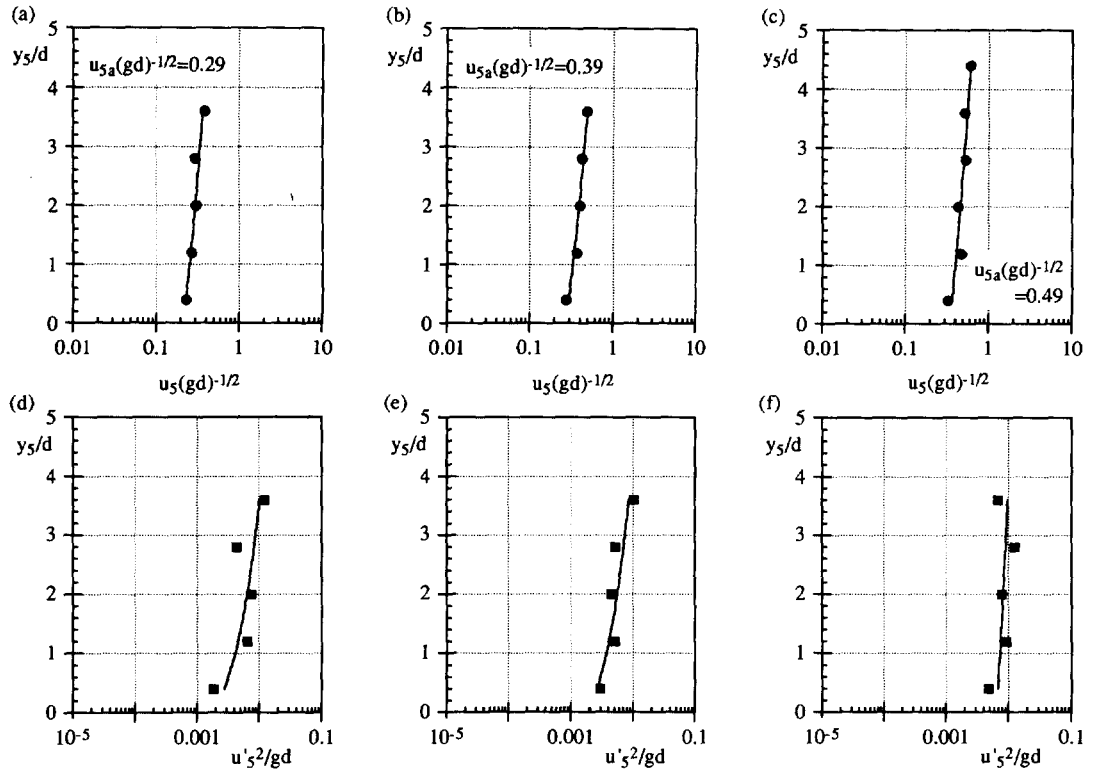

Figure 9. Measurements ($u_s = 3.07$ m/s). (a) particle velocity at $x_5 = 5.3$ mm; (b) particle velocity at $x_5 = 12.7$ mm; (c) particle velocity at $x_5 = 18.4$ mm; (d) granular temperature at $x_5 = 5.3$ mm; (e) granular temperature at $x_5 = 12.7$ mm; (f) granular temperature at $x_5 = 18.4$ mm.

If we assume that the mass flux of the particle phase in the granular bed towards the jet is independent of y_5 it follows that the axial particle flux in the jet (mixing region 1; see figure 1) increases linearly from zero to the final value

$$\alpha_2 \rho_p b u_{pc} 2 \int_0^{1/2} \frac{u_p}{u_{pc}} \, \mathrm{d}\frac{y_2}{b} = \begin{cases} \dot{m}_p, & x_2 \geqslant h \\ \dfrac{\dot{m}_p}{h} x_2, & x_2 < h. \end{cases} \qquad [4]$$

In [4] $\dot{m}_p$ denotes the mass flux of particles per unit depth which has been taken from experiments by multiplying the measured value u_{5a} (figure 11) for the lowest superficial velocity $u_s = 1.47$ m/s with the height h of the granular bed, the density of the particles $\rho_p = 2400$ kg/m^3 and an estimated value for $\alpha_5 = 0.55$:

$$\dot{m}_p = 2 u_{5_z} \alpha_5 \rho_p h. \qquad [5]$$

The importance of various possible modes of particle–fluid interactions in the vicinity of the orifice is not clear and no attempt was made to incorporate them into the present model. From visual observations it appears that shear induced lift and Magnus forces are of some importance (Melville and Bray 1979).

As shown in figure 12 the particle velocity inside the jet can be represented by a Gaussian distribution. Thus, we assume that this is also true for the fluid phase and we write

$$\frac{u_f}{u_{fc}} = \frac{u_p}{u_{pc}} = \mathrm{e}^{-ky^2}, \qquad [6]$$

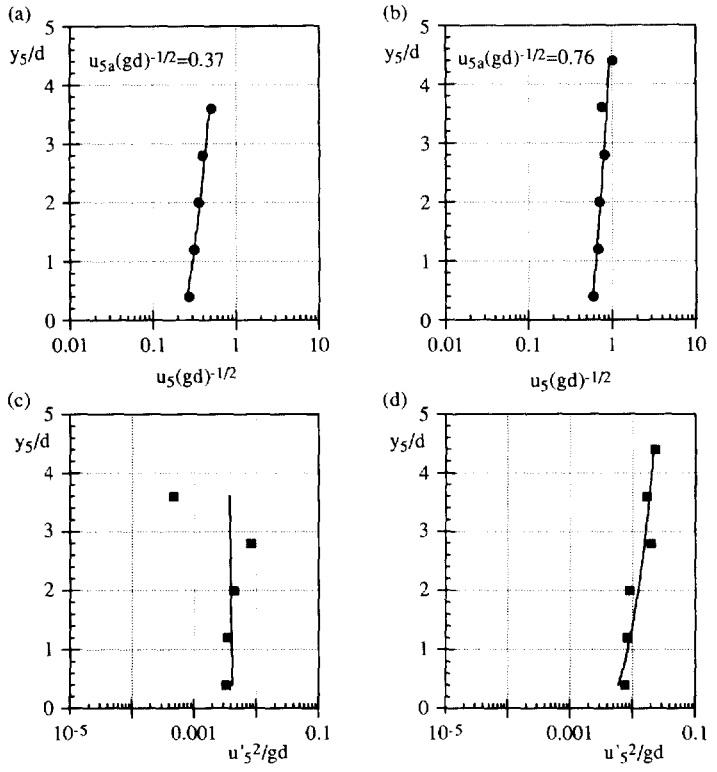

Figure 10. Measurements ($u_s = 4.50$ m/s). (a) particle velocity at $x_5 = 12.7$ mm; (b) particle velocity at $x_5 = 18.4$ mm; (c) granular temperature at $x_5 = 12.7$ mm; (d) granular temperature at $x_5 = 18.4$ mm.

where the parameter k is calculated from the measured conditions at the jet edge given by the observed spreading angle Θ,

$$u_p\Big|_{z=\pm\frac{b}{2}} = 0.2u_{pc} \qquad [7]$$

The velocity profiles of both phases are self-similar when scaled with the distance from the virtual jet origin. For a measured spreading angle $\Theta = 28^\circ$, the virtual origin is at $x_v = -2b_0$ (figure 13).

Due to similarity of the velocity profiles all the integrals in [1], [2] and [4] are reduced to two different constants which are determined by the parameter k. Then, [1] and [2] the volume concentration α_2 was eliminated by means of [4]. Eventually, a method of finite differences was

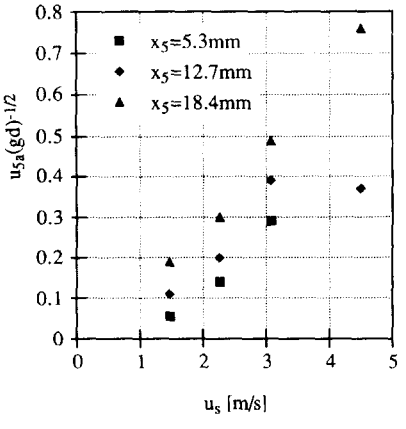

Figure 11. Mean particle velocity u_{5a} vs superficial velocity u_s.

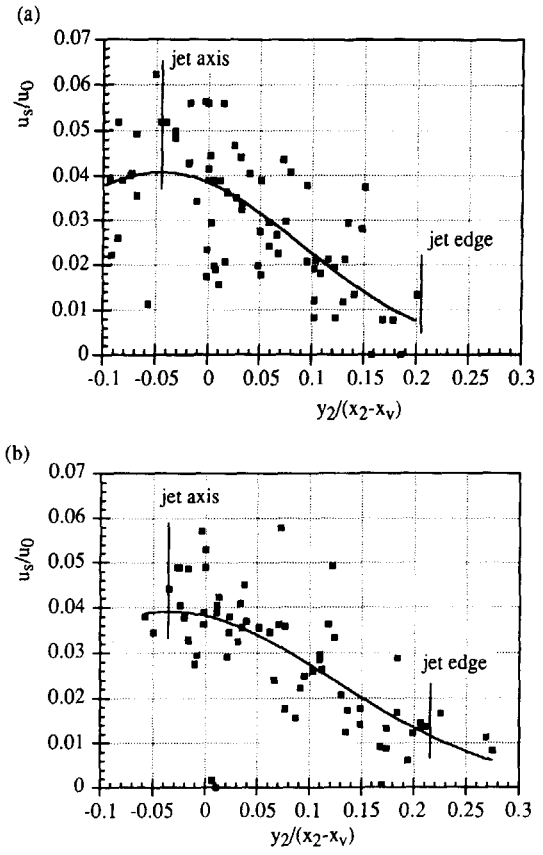

Figure 12. Particle velocities within the jet. (a) $x_2/b_0 = 5.4$; (b) $x_2/b_0 = 3.3$.

applied to solve the resulting system of two non-linear ordinary differential equations for the velocity at the centerline u_{pc} and u_{fc} for a given air velocity u_0 at the orifice. Subsequently, the volume concentration α_2 follows from [4].

In table 1 the experimental parameters which were used for calculating the velocity and the concentration within the jet are presented. Since the mass flux of particles $\dot{m}_p$ was assumed to be constant for all experimental runs, the volume concentration α_5 in the granular flow was calculated from the measured value of the average particle velocity u_{5a} (figure 11). Here we note that the

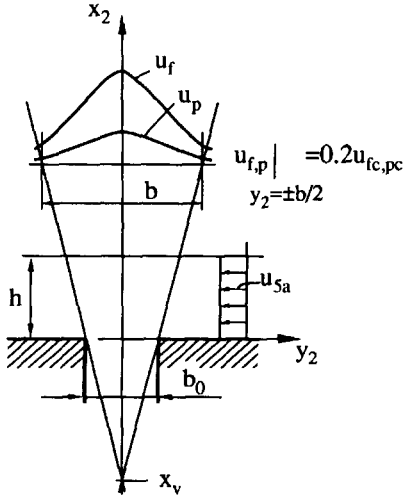

Figure 13. Sketch of the jet model.

Table 1. Parametric values

u_s [m/s]	u_0 [m/s]	h [mm]	c_{d_z}	α_S
1.47	10.5	8.0	0.5	0.55
2.26	16.0	6.6	0.5	0.42
3.07	22.0	6.6	0.4; 0.5	0.26

$b_0 = 7$ mm; $d_p = 1.5$ mm; $\Theta = 28°$; $\dot{m}_p = 0.48$ kg/ms
$\rho_p = 2400$ kg/m^3; $\rho_f = 1.21$ kg/m^3.

experimentally obtained values of α_S are in reasonable agreement with the calculations to be presented in section 4.

Figures 14–18 show the numerical results according to the parameters obtained from experiments. In figures 14–16 the dimensionless center velocity u_{pc}/u_0 and the volume concentration α_2 are plotted as a function of x_2/b_0. From experimental observation we assumed the volume concentration of particles in the surroundings of the jet (region 4, see figure 1) to be either zero (figure 14) or equal to α_2 (figures 15, 16). In all cases, the volume concentration α_2 increased within the mixing region according to [4]. The following spreading of the jet caused a decrease of α_2 until the volume concentration became almost constant over a wide range of x_2/b_0, a results confirmed by all experiments (figures 3–6). Finally, the air velocity became too small in order to further accelerate the particles which caused α_2 to increase sharply. This fact made the assumptions for the model invalid. For a relatively small superficial velocity (figure 14) this breakdown occurred before the particles reached the tube ($x_2/b_0 \sim 5$). This theoretical prediction was in good agreement with the experimental observation (figure 3) from which we estimated $x_2/b_0 \sim 6$. In figure 16 we varied the value of c_{d_z}. Apparently, the drag coefficient is a very crucial parameter and $c_{d_z} = 0.4$ yields better agreement with measurements than $c_{d_z} = 0.5$. However, if one takes into account the roughness of the model, overall agreement is reasonable. Figure 17 shows numerical results for the centerline velocity u_{fc}/u_0 as a function of x_2/b_0 and with the superficial velocity u_s as a parameter. The initial increase of u_{fc}/u_0 for $u_s = 1.47$ m/s is due to relatively strong buoyancy within the mixing region.

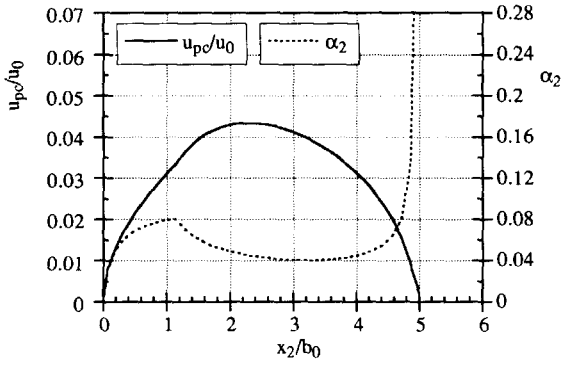

Figure 14. Particle centerline velocity and volume fraction ($u_s = 1.47$ m/s).

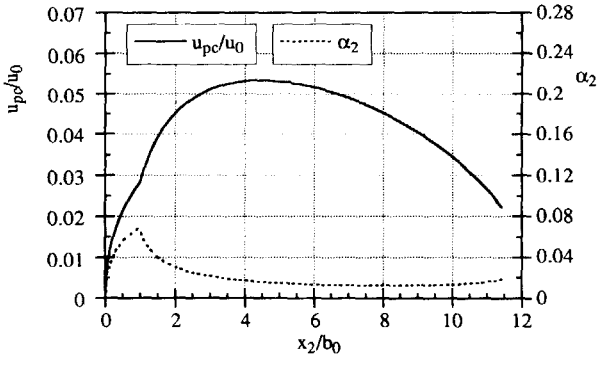

Figure 15. Particle centerline velocity and volume fraction ($u_s = 2.26$ m/s).

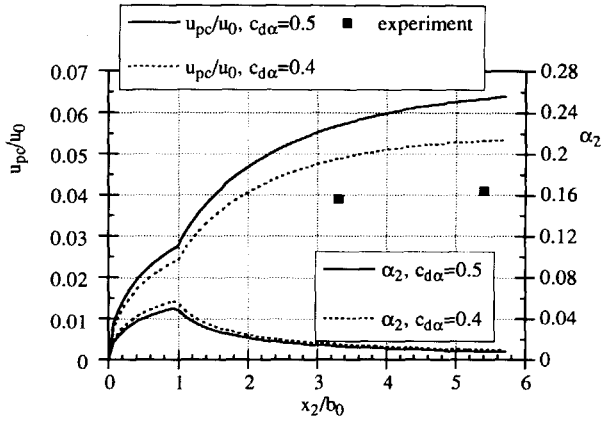

Figure 16. Particle centerline velocity and volume fraction (u_s = 3.07 m/s).

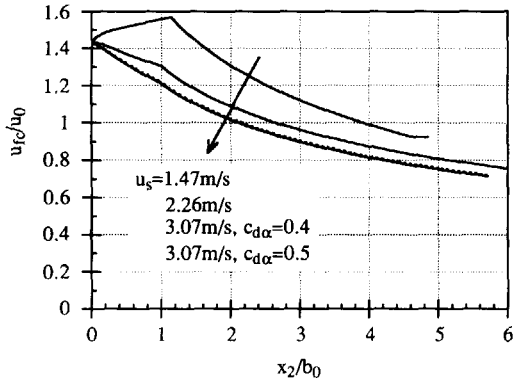

Figure 17. Centerline fluid velocities.

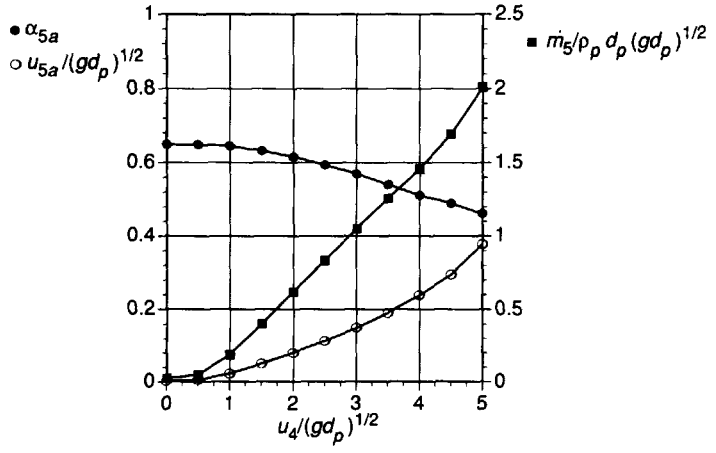

Figure 18. Average particle volume concentration, velocity, and mass flux as a function of the velocity $u_4/(gd_p)^{1/2}$.

Table 2. Physical parameters used in the present calculations

e_p	grain–grain coefficient of restitution	0.89
e_w	grain–wall coefficient of restitution	0.87
d_p	particle diameter	0.15 cm
ρ_p	particle density	2.4 g/cm^3
β	inclination angle	15
A	dimensionless height of the layer (H/d_p)	5.0

The impingement rate per unit depth N [m^{-1} s^{-1}] is needed to further investigate the impingement region 3 (see figure 1) and the defrosting mechanism. N can be easily estimated from the jet quantities, the jet width and the geometry of the tube:

$$N = \frac{\dot{m}_p \int_0^{R/b} \frac{u_p}{u_{p_c}} \, \mathrm{d}\frac{y_2}{b}}{m_{sp} \int_0^{1.2} \frac{u_p}{u_{p_c}} \, \mathrm{d}\frac{y_2}{b}}. \qquad [8]$$

In [8], m_{sp} is the mass of one particle and R is the radius of the heat exchanger tube. With the width of the jet at the heat exchanger tube $b/b_0 = 3.86$, the given mass flux of particles $\dot{m}_p = 0.48$ kg/s and for a superficial velocity $u_s = 3.07$ m s^{-1}, the impingement rate $N \sim 100\,000$ m^{-1} s^{-1}.

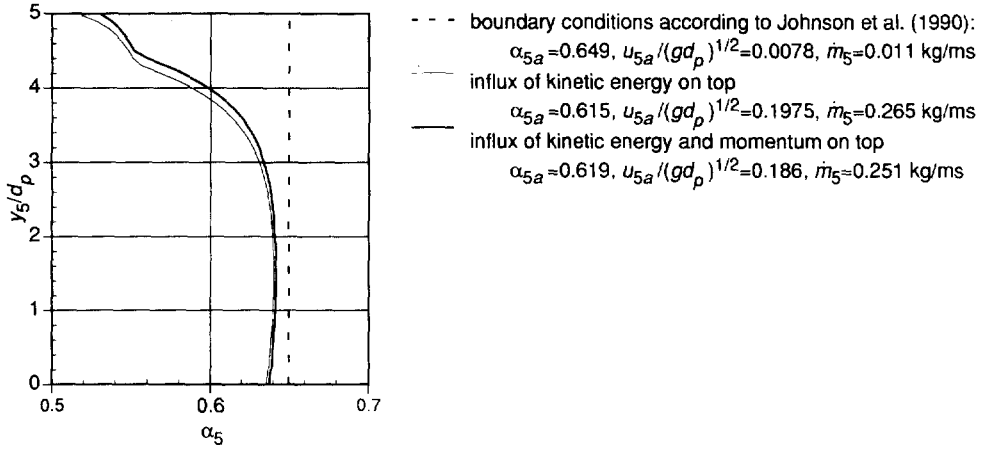

Figure 19. Volume concentration profiles for different boundary conditions on top.

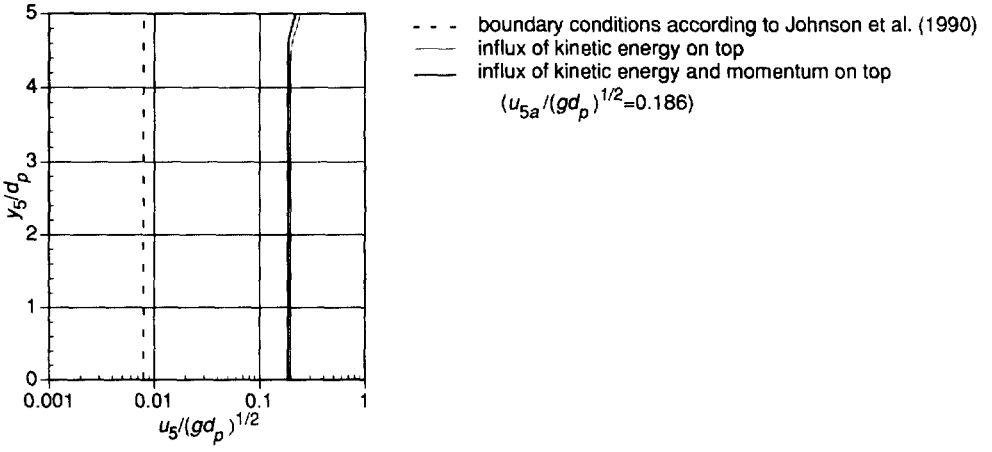

Figure 20. Velocity distribution for different boundary conditions on top.

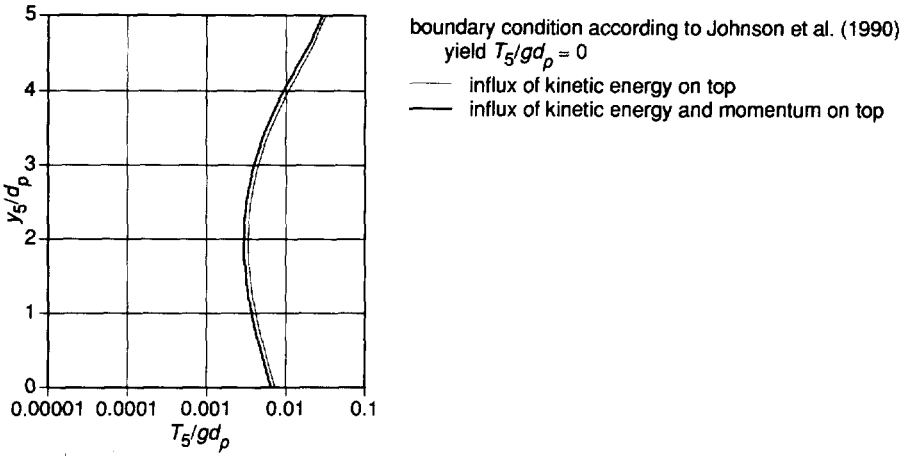

Figure 21. Granular temperature for different boundary conditions on top.

4. GRANULAR FLOW

Johnson *et al.* (1990) developed a theoretical model to calculate the granular flow on chutes. The theory is based on rheological criterions for the material, which take into account both collisional and frictional mechanisms for the granular stress. Even though such a theory cannot predict all experimentally observed phenomena, numerical results for the problem under investigation at least provide important information about the influence of material properties such as the coefficient of restitution (see table 2) on the flow quantities. Since this section mainly follows the paper by Johnson *et al.* (1990), we recapitulate their frictional-collisional model here and discuss in detail modified boundary conditions on top of the granular bed for both the granular temperature T and the stress. These boundary conditions account for the additional contribution to kinetic energy and momentum by the surroundings region 4 (see figure 1). The governing equations for continuity, momentum and granular temperature are:

$$\frac{D\rho_5}{Dt} + \rho_5 \nabla \cdot \mathbf{u}_5 = 0, \qquad [9]$$

$$\rho_5 \frac{D\mathbf{u}_5}{Dt} = \rho_5 \boldsymbol{g} - \nabla \cdot (\sigma_f + \sigma_c) \qquad [10]$$

$$\frac{3}{2} \rho_5 \frac{DT}{Dt} = -\nabla \cdot \mathbf{q}_{PT} + \sigma_c : \nabla \cdot \mathbf{u}_5 - I. \qquad [11]$$

In the equations above ρ_5 is the bulk density of solid particles. The symbols σ_f and σ_c refer to the stress in the granular material due to friction and collision, respectively. The gravitational constant is denoted by $\boldsymbol{g}$, while $\mathbf{u}_5$ is the mean velocity as already defined earlier. Equation [11] is a local balance of pseudo-thermal energy given by the flux divergence $\nabla \cdot \mathbf{q}_{PT}$, the rate of generation due to shearing $-\sigma_c : \nabla \cdot \mathbf{u}_5$ and the rate of dissipation/volume I due to inelastic collisions. It should be noted that the latter quantity depends on the particle–particle coefficient of restitution e_p.

According to Johnson *et al.* (1990) the boundary condition for the relative (slip) velocity $\mathbf{u}_{sl} = (\mathbf{u}_5 - \mathbf{u}_{wall})$ at a wall can be derived from the stress exerted by the moving particles on solid boundaries:

$$(\sigma_f + \sigma_c) \cdot \frac{\mathbf{u}_{sl}}{|\mathbf{u}_{sl}|} \cdot \mathbf{n} + \frac{\phi^* \pi \rho_p \alpha_5 \sqrt{3T}}{6\alpha_{max}\left[1 - \left(\frac{\alpha_5}{\alpha_{max}}\right)^{1/3}\right]} |\mathbf{u}_{sl}| + N_f \tan\delta = 0. \qquad [12]$$

Here $\mathbf{n}$ is the unit normal vector directed from the boundary into the material. The maximum solid fraction of particles for random packing is assumed to be $\alpha_{max} = 0.65$. The first term in [12] represents the limit of the stress in the material on approaching the boundary, while the second and third terms account for the stress acting on the boundary caused by particle–wall collisions and friction, respectively. The second term is proportional to a coefficient ϕ^*, defined as the average fraction of relative tangential momentum transferred in a particle-boundary collision. The magnitude of the tangential frictional contribution to the stress is assumed to be $N_f \tan\delta$, where N_f is the normal frictional component of stress and δ is the angel of friction between the surface and the solid particles.

Another boundary condition at the wall is the flux of pseudo-thermal energy, which equals the difference between the rate of pseudo-thermal energy dissipation/area due to inelastic particle–wall collisions, $\mathscr{D}$, and the rate of energy generation that occurs as particles slip along the boundary, i.e.

$$-\mathbf{n}\cdot\mathbf{q}_{PT} = \mathscr{D} + \mathbf{u}_{sl}\cdot\frac{\phi^*\pi\rho_p\alpha_5\sqrt{3T}}{6\alpha_{max}\left[1-\left(\frac{\alpha_5}{\alpha_{max}}\right)^{1/3}\right]}|\mathbf{u}_{sl}| \qquad [13]$$

with

$$\mathscr{D} = \frac{\pi(1-e_w^2)\rho_p\alpha_5 T\sqrt{3T}}{4\alpha_{max}\left[1-\left(\frac{\alpha_5}{\alpha_{max}}\right)^{1/3}\right]}, \qquad [14]$$

where e_w is the particle wall coefficient of restitution.

Equations [12] and [13] provide *ad hoc* expressions that are reasonably faithful to situations where both frictional and collisional mechanisms of stress generations are significant. More rigorous boundary conditions for rapid granular flow were derived by Jenkins (1992) and later improved by Louge (1994) and Louge and Jenkins (1994).

Furthermore, we need additional stress and pseudo-thermal energy boundary conditions at the free surface on top. An energy balance at the surface requires that the flux of pseudo-thermal energy is equal to the pseudo-thermal energy transferred to the granular bed by particle emotion in the surroundings region 4 (see figure 1):

$$-\mathbf{n}\cdot\mathbf{q}_{PT} = \frac{\dot{m}_p\mathbf{u}_4^2}{4L}. \qquad [15]$$

The velocity $\mathbf{u}_4$ can be estimated by the observed equal volume concentration of solids inside the jet and the surroundings (see figures 4 and 5).

The stress condition at the surface simply follows from the force on the particles adjacent to the top:

$$\frac{\pi\rho_p d_p \mathbf{g}}{6\left(\frac{\alpha_{max}}{\alpha_5}\right)^{2/3}} + \phi\frac{\dot{m}_p\mathbf{u}_4}{2L} = \mathbf{n}\cdot(\sigma_f + \sigma_c). \qquad [16]$$

In [16] the normal total stress caused by friction and collision multiplied with the area occupied per particle is equal to the volume force caused by gravity acting on a single particle and the additional influx of momentum from the surroundings. The coefficient ϕ varies between 0 and 2 and represents the fraction of momentum which is transferred to the top layer. Since nothing is known about an actual value of ϕ we simply assumed $\phi = 1$. This assumption is justified by the fact that at the top a certain fraction of falling particles bounce back while the rest of particles move rather unhindered into deeper layers of the granular bed.

With the constitutive equations for σ_f, σ_c, $\mathbf{q}_{PT}$, and I as given by Johnson *et al.* (1990) and for a fully developed steady flow, [9]–[16] are reduced to a system of ordinary differential equations, which were solved numerically using a standard Runge–Kutta procedure.

Except for particle and wall materials (restitution coefficients e_p, e_w, particle diameter d_p and particle density ρ_p) the physical parameters were the same as chosen by Johnson *et al.* (1990). In our case the bottom wall was acrylic plastic and therefore we assumed e_w being smaller than the value for smooth aluminum (Johnson *et al.*, 1990). From experimental observations we also inferred that the grain–grain coefficient of restitution e_p was slightly smaller than the value used by Johnson *et al.* (1990). Table 2 not only depicts the values of parameters which differ from those chosen by Johnson *et al.* (1990) but also includes the geometric parameters for the present chute.

Figure 18 gives the results of a parametric study with the purpose to obtaining a reasonable value for the influx velocity u_4. For a given mass flux $\dot{m}_p/2 = 0.24$ kg.ms, figure 18 yields $u_4 = 0.23$ m/s, a value which is in good agreement with experimental observations. In addition, figure 18 provides information about the average particle volume concentration α_{5a} and the average particle velocity u_{5a}. Figure 19 depicts the concentration profiles for various boundary conditions on the top. The dashed line represents the solution according to Johnson *et al.* (1990). The particles remain near maximum concentration and thus hardly move at all as long as there is no influence of kinetic energy and momentum on top of the granular layer.

As one expects, the influx of kinetic energy alone (figure 19, thin line) causes the particles to be slightly less dense than when there is also additional input of momentum (figure 19, thick line), which compresses the particles. As a result, the incoming mass flux from the surroundings $\dot{m}_4$ equals, to a good degree, the mass flux $\dot{m}_5 = \dot{m}_p/2$ within the granular bed only if the boundary conditions [16] and [17] are satisfied. This fact clearly shows the necessity of implementing the full boundary conditions [16] and [7].

The velocity distribution is shown in figure 20. Again, the dashed line indicates that there is practically no flow for boundary conditions according to Johnson *et al.* (1990). The full lines, however, are in good agreement with the measured velocity distribution as shown in figure 8(b).

The comparison between the measured granular temperature, figure 8(e), and the appropriate calculations, figure 21, also shows excellent agreement. For ordinary boundary conditions at the top (Johnson *et al.* 1990) the granular temperature is close to zero. Again, only the influx of kinetic energy and momentum on top of the granular layer causes the particles to flow as observed in the experiments.

5. CONCLUSIONS

We presented here a theoretical approach to studying the two-phase jet and the granular flow of particles in a very shallow fluidized bed (Aihara *et al.* 1995). First, high speed video recordings were evaluated in order to obtain data for the velocity distribution within the granular layer which forms on the inclined bottom wall. The videos also helped provide data for the average mass flux of particles. We kept this mass flux constant throughout the present investigation at a value consistent with our observations. We were also able to estimate the granular temperature from the velocity fluctuations. In addition, we measured the angle of the two-phase jet which quickly forms in the mixing region, and we measured the particle velocity within the jet.

Second, we calculated the centerline velocities of the two phases and the average volume concentration of particles within the jet. Both results led to an estimate for the average impingement rate of particles on the heat exchanger tube. This theoretical approach was based on conservation of overall momentum and the assumption that momentum transfer between the two phases is due to interaction by drag and gravity. For both, air and particles, we assumed a Gaussian velocity distribution within the jet.

The numerical results showed that the average particle volume concentration remained nearly constant over a wide range of distance. This fact was indeed clearly observed in all experiments. The measured centerline velocity was, however, only in fair agreement with the theoretical predictions since the calculation is very sensitive to the value of the drag coefficient, which is not precisely known.

Third, we investigated the granular flow of the particles sliding on the inclined bottom wall. The analysis was founded on a theoretical model introduced by Johnson *et al.* (1990). In the present case, however, we had to modify the boundary conditions on top of the layer in order to account for the additional influx of kinetic energy and momentum from above. It turned out that this influx

had a strong influence and was the driving source for the particle flow within the granular layer. For the parameter values given in table 2, the numerical solutions were in excellent agreement with the measurements.

So far no attempts were made to study theoretically the two-phase flow in the surroundings of the jet and the granular layer. In that region the particles settle due to gravity, but are also strongly influenced by the neighboring jet and the heat exchanger tubes. Only if the particles impinged on to the heat exchanger tube (figures 4–6) we experimentally observed that the volume concentration of particles within the surroundings was practically the same as within the jet.

Acknowledgements—The authors are grateful to Mr T. Shimoyama who contributed to this paper with his experimental expertise. The authors also thank one referee for recommending further literature on this subject. This work was supported by a Grant-in-Aid for International Scientific Research Program No. 06044018 from the Ministry of Education, Science and Culture of Japan.

REFERENCES

Aihara, T., Maruyama, S., Hongoh, M. and Aya, S. (1988) Heat transfer and pressure loss of a very shallow fluidized-bed heat exchanger. Part 1: Experiment with a single row of tubes. *Experimental Thermal and Fluid Science* **1,** 315–323.

Aihara, T., Ohara, T., Shimoyama, T. and Kitano, H. (1995) Heat-transfer and defrosting characteristics of a horizontal array of cooled tubes immersed in a very shallow fluidized bed. *Int. J. Heat & Mass Transfer* (submitted).

Aoki, K., Hattori, M. and Itoh, T. (1985) A study of extended surface heat exchanger with frosting (1st report, overall heat transfer characteristics). *Trans. JSME, Ser. B* **51,** 3048–3054 (in Japanese).

Fukusako, S., Ishiguro, S. and Seki, N. (1985) Heat-transfer characteristics from a bundle of horizontal tubes immersed in aggregative fluidized bed. *Wärme- und Stoffübertragung* **22,** 13–22.

Fukusako, S., Tago, M., Yamada, M., Ozaki, M., Torikoshi, K. and Kawabata, K. (1989) Frosting heat transfer from a bundle of horizontal tubes immersed in aggregative fluidized bed. In *Heat Transfer with Phase Change*, eds I. S. Habib and R. J. Dallman. ASME HTD Vol. 114, pp. 29–37.

Hayashi, Y., Aoki, K. and Yuhara, H. (1977) Study of frost formation based on a theoretical model of the frost layer. *Heat Transfer Japanese Res.* **6,** 79–94.

Jenkins, J. T. (1992) Boundary conditions for rapid granular flows: flat, frictional walls. *J. of Appl. Mech.* **59,** 120–127.

Johnson, P. C., Nott, P. and Jackson, R. (1990) Frictional–collision equations of motion for particulate flows and their application to chutes. *J. Fluid Mech.* **210,** 501–535.

Laats, M. K. and Frishman, F. A. (1970) Assumptions used in calculating the two phase jet. *Fluid Dynamics* **5,** 333–338.

Louge, M. Y. (1994) Computer simulations of rapid granular flows of spheres interacting with a flat, frictional boundary. *Phys. Fluids* **6,** 2253–2269.

Louge, M. Y. and Jenkins, J. T. (1994) Boundary conditions for rapid flows of inelastic frictional spheres in sliding collisions with a flat frictional wall. *Fluidization and Fluid–Particle Systems*, special supplement to the fall annual meeting, AIChE, NY, p. 7.

Maruyama, S., Aihara, T., Tanaka, Y. and Kasahara, K. (1988) Heat transfer and pressure loss of a very shallow fluidized-bed heat exchanger. Part 2: Experiment with multirow tube banks. *Experimental Thermal and Fluid Science* **1,** 325–333.

Maruyama, S., Aihara, T., Tanaka, Y. and Kasahara, K. (1989) Development of an air-cooled bare-tube condenser utilizing low pressure-loss fluidized bed for heat-pump systems. *Trans. Soc. Air Conditioning and Sanitary Eng. of Japan* **40,** 57–63 (in Japanese).

Melville, W. K. & Bray, K. N. C. (1979) A model of the two-phase turbulent jet. *Int. J. Heat Mass Transfer* **22,** 647–656.

Mostafa, A. A., Mongia, H. C., McDonell, V. G. and Samuelsen, G. S. (1989) Evolution of particle-laden jet flows: a theoretical and experimental study. *AIAA Journal* **27,** 167–183.

Richardson, J. F. and Zaki, W. N. (1954) Sedimentation and fluidization: Part I. *Trans. Inst. Chem. Engrs* **32,** 35–53.

Schneider, W. (1985) Decay of momentum flux in submerged jets. *J. Fluid Mech.* **154,** 91–110.

Seki, N., Fukusako, S., Matsuo, K. and Uemura, S. (1985) An analysis of incipient frost formation. *Wärme- und Stoffübertragung* **19,** 9–18.

Torikoshi, K., Kawabata, K. & Yamashita, H. (1990) Heat transfer from a tube immersed in a fluidized bed with frosting. *Heat Transfer Japanese Res.* **19,** 73–91.

Wallis, G. B. (1969) *One-dimensional Two-phase Flow.* McGraw-Hill, New York.

Yamakawa, N., Takahashi, N. and Ohtani, S. (1972) Forced convection heat and mass transfer under frost condition. *Heat Transfer Japanese Res.* **1,** 1–10.

Zierfuss, R. and Schneider, W. (1992) Jet flows in fluidized beds. *Z. Angew. Math. u. Mech.* **72,** T398–T400.